GEOTECHNICAL CHALLENGES IN KARST

ISRM Specialised Conference / Međunarodna konferencija
8. Savjetovanje Hrvatskog geotehničkog društva
Omiš – Split, Croatia, 11.-13.04.2019.
ISBN 978-953-95486-8-9

Deep Tunnels, Cliffs, Mountain Walls and Mountains: An Exploration of Failure Modes in Rock and Rock masses

Duboki tuneli, klifovi, litice i planine: istraživanje modela loma u stijenama i stijenskim masama

Nick BARTON[1]

Abstract

In relation to soil, rock is usually extremely strong, with a compression strength that will seldom be mobilized, even in deep tunnels. Intact rock may also have cohesion that is so high that it makes mountain avalanches rare events. Frictional strength tends to be high as well, due to the big contribution of dilation unless the rock has high porosity. The weakest link of the intact rock is of course it's tensile strength. It is realized now that Poisson's ratio also plays a major role in failure, as even rock under 3D compression can fail in tension due to the mechanism of extensional strain in the direction of a free surface. This is an important morphological property. Naturally if the rock is jointed, there are usually massive changes in strength and stability and slope height, in relation to slopes in intact rock. Failure may be progressive in nature, involving several components. In this paper all these aspects will be explored utilizing deep tunnels, and then the maximum heights of cliffs and mountain walls. The apparent 8 to 9km height limit of mountains will also be addressed using critical state shear strength arguments, since confined compression strength is too high.

Keywords: **Extensional strain, shear strength criteria, deep tunnels, mountain walls, mountain heights**

Sažetak

U odnosu na tlo, stijene su uobičajeno iznimno velike čvrstoće, s tlačnom čvrstoćom koja se rijetko dostiže, čak i u dubokim tunelima. Intaktna stijena također može imati i koheziju koja je toliko visoka da se planinske lavine događaju rijetko. I trenje teži visokim vrijednostima zbog velikog doprinosa dilatancije, osim u slučaju stijena visoke poroznosti. Najslabija karika intaktne stijene je, naravno, njezina vlačna čvrstoća. Prema novijim saznanjima, i Poissonov omjer ima važnu ulogu u pojavi loma, jer se čak i u stijeni u uvjetima 3D kompresije može dogoditi vlačni lom uslijed mehanizma razvoja vlačnih deformacija u smjeru slobodne površine. To je važno morfološko svojstvo. Naravno, ako su u stijeni prisutni diskontinuiteti, uglavnom postoje znatne promjene čvrstoće, stabilnosti i visine padine u odnosu na padine u intaktnoj stijeni. Lom po prirodi može biti progresivan, uključujući nekoliko komponenti. U ovom radu će se istražiti svi ovi aspekti koristeći duboke tunele, a potom i najveće visine klifova i litica. Očigledno ograničenje visine planine na 8 do 9 km također će se obrazložiti koristeći argumente kritičnog stanja posmične čvrstoće, budući da je tlačna čvrstoća u uvjetima spriječenog širenja previsoka.

Ključne riječi: **Vlačna relativna deformacija, kriterij posmične čvrstoće, duboki tuneli, litice, visine planina**

[1] NB&A, Oslo, Norway, nickrbarton@hotmail.com

Failure in deep tunnels

Two empirical methods for assessing the onset of fracturing in deep tunnels in massive rock represent the starting point for this wide-reaching exploration of failure modes and the 'strength' of rock masses. Since we will first consider massive or unjointed rock in deep tunnels, we can utilize the classical (Kirsch) formulation for estimating the maximum tangential stress ($\sigma_{\theta\ max}$) in two diametrically opposite locations surrounding an idealized circular tunnel cross-section, excavated or bored in an isotropic elastic medium: ($\sigma_{\theta\ max} = 3\sigma_1 - \sigma_3$).

Table 1 illustrates an SRF (stress reduction factor) table from the Q-system (Grimstad and Barton, 1993) for comparison with a later, closely related 'depth-of-failure' figure from Martin et al. 1998 shown in Figure 1.

Table 1.The sixth Q-parameter: SRF adjusts the Q-value for the effect of adverse (or benign) ratios of tangential stress in relation to uniaxial strength.

	b) Competent rock, rock stress problems	σ_c/σ_1	σ_θ/σ_c	**SRF**
H	Low stress, near surface, open joints.	> 200	< 0.01	2.5
J	Medium stress, favourable stress condition.	200-10	0.01-0.3	1
K	High stress, very tight structure. Usually favourable to stability, may be unfavourable for wall stability.	10-5	0.3-0.4	0.5-2
L	Moderate slabbing after > 1 hour in **massive** rock.	5-3	0.5-0.65	5-50
M	Slabbing and rock burst after a few minutes in **massive** rock.	3-2	0.65-1	50-200
N	Heavy rock burst (strain-burst) and immediate dynamic deformations in **massive** rock.	< 2	> 1	200-400

Table 1 and Figure 1 (top) are telling us the same story from independent sources: expect failure when reaching and passing a maximum tangential stress/unconfined strength ratio ($\sigma_{\theta\ max}/\sigma_c) = 0.4 \pm 0.1$. The photographs in Figure 1 show fully developed log-spiral shearing in a sandstone model (Addis et al. 1990) and fracture initiation in a TBM tunnel in marble.

These are examples of the propagation of initial extension fracturing into shearing, which may become unstable signalling the possibility of rock bursts at even higher stress levels (Shen and Barton, 2018).

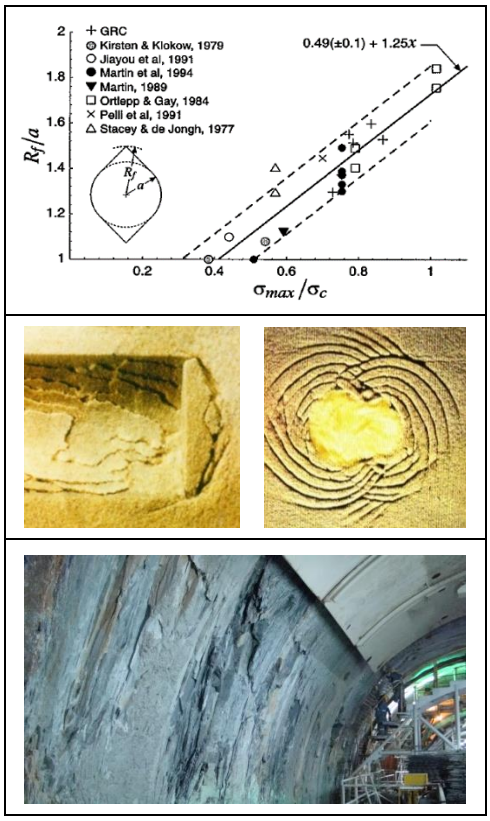

Figure 1. The accelerating SRF ratings (giving lower Q and more reinforcement) when the ratio σ_θ/σ_c reaches and exceeds 0.4 (Table 1) is matched by the independently derived mining and nuclear waste research data concerning depth of fracturing (R_f -a) from Martin et al. 1998.

As will be seen from Figure 2, the critical tangential stress can alternatively be expressed as (σ_t/ν). If we assume typical ratios of uniaxial compression/tensile strength (σ_c/σ_t) of 10, and typical values of Poisson's ratio (ν) of 0.25, simple arithmetic shows that the ratio of tensile strength and Poisson's ratio (σ_t/ν) is equal to $0.4 \cdot \sigma_c$. This is the same approximate stress/strength ratio seen when acoustic emission begins to increase in laboratory tests.

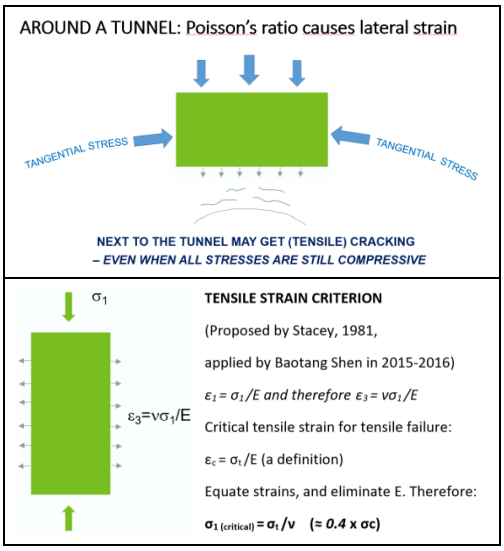

Figure 2. An imaginary rock sample in the arch of a deep tunnel, subjected to a horizontal maximum tangential stress in the arch due to high horizontal stress. Baotang Shen was responsible for noticing the critical stress-strain interpretation which explains the familiar ratio of stress/strength of 0.4. (See Shen and Barton, 2018 for more detail).

Figure 3 shows the FRACOD modelling of a 'stressed' (and strained) TBM tunnel, with initial extension fractures propagating in shear. The massive wall failures in this earliest of TBM tunnels occurred due to an unusually abrupt increase in stress (+ strain).

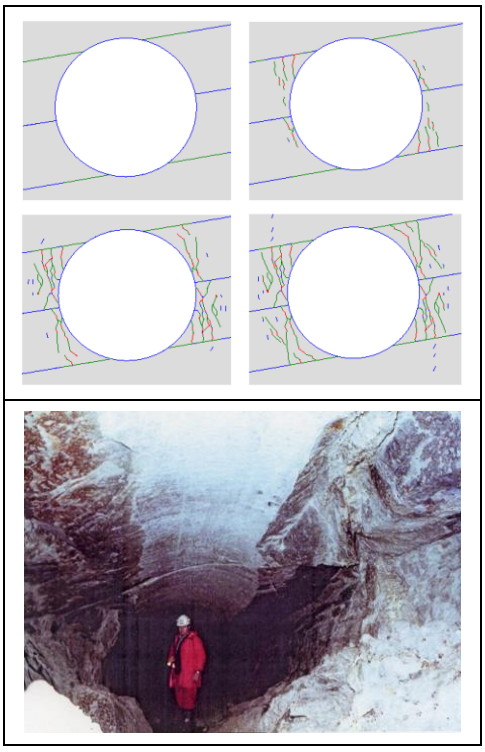

Figure 3 The Beaumont (or English) Tunnel driven in 1880, showing failure in the 8 to 10 o'clock and 2 to 4 o'clock locations due to an increase in vertical stress when this earliest TBM tunnel (in chalk marl) passed under the 70m high Shakespeare Cliffs (UK). The FRACOD modelling with assumed horizontal-to-vertical stress ratio of 1/3 was performed by Baotang Shen. (Barton and Shen, 2017).

Theoretical heights of cuttings and cliffs

We will now consider the stability and failure modes exhibited at the surface, firstly for the case of cuttings in soil, then address cliffs (in weaker rock) and mountain walls (in stronger rock). In place of the Kirsch equations for tangential stress concentrations surrounding circular TBM-like excavations, we can now consider the local principal vertical stress behind a cutting or cliff or mountain wall. This can be compared with a measure of the strength of the soil or rock in the same way as before.

The likelihood (or not) of failure along an inclined shear surface exiting at the toe of the slope will also be assessed. Both the stability of steep cuttings (in soil) and the stability of (sea and river) cliffs in rock might at first sight appear to be governed by conventional Mohr-Coulomb based shear resistance involving cohesion (c) and friction angle (φ), but with differentiation of these strength parameters to allow for the weakness of soil and the relative strength of most rocks.

Soil mechanics text books show lower-bound and upper-bound solutions for the

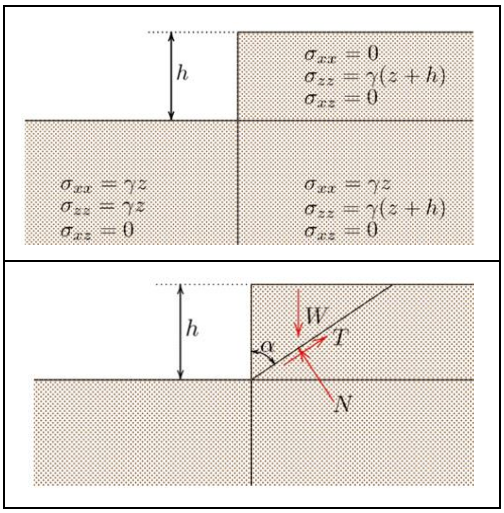

Figure 4. Top: The equilibrium assumptions for the three zones gives a lower-bound solution. Bottom: An assumed planar shear surface gives an upper-bound solution. The critical height (h) therefore varies between wide margins $4c/\gamma \tan(45° + \varphi/2) \geq h \geq 2c/\gamma \tan(45° + \varphi/2)$ with a circular failure surface giving a solution closer to the upper-bound with a multiplier of 3.85. Verujit, 2001.

stability of vertical cuttings, based on c and also φ, utilizing the two different assumptions illustrated in Figure 4.

Equations 1 and 2 summarize the limits of the soil-based criteria. It seems that an exact solution to the vertical cutting problem is elusive, even when utilizing a linear Mohr-Coulomb strength envelope. In the case of high mountain walls one would need a stress dependent 'Mohr-Coulomb' modification. However, as we shall see, the weakest link that actually determines the maximum height of cliffs or mountain walls in (intact) rock depends on two entirely different parameters than c and φ.

$$h \geq 2c/\gamma \ tan(45° + \varphi/2) \quad (1)$$

$$h \leq 4c/\gamma \ tan(45° + \varphi/2) \quad (2)$$

If we do a trial evaluation of potential c and φ values for intact rock, using a lower-bound estimate of cohesion from equation 3 shown below Figure 5, we find very quickly that the soil-cutting based solutions of Figure 4 that work for soil with its relatively low cohesion, *result in far too high values of critical height* (i.e. the maximum possible vertical height) in a range of rocks we are familiar with. The cohesive strength of intact rock is apparently too high unless the vertical slopes are very high, Experience suggests *alternative failure modes* kicking in at smaller cliff or wall heights: in fact failure is due to *extensional strain*, or the involvement of jointing.

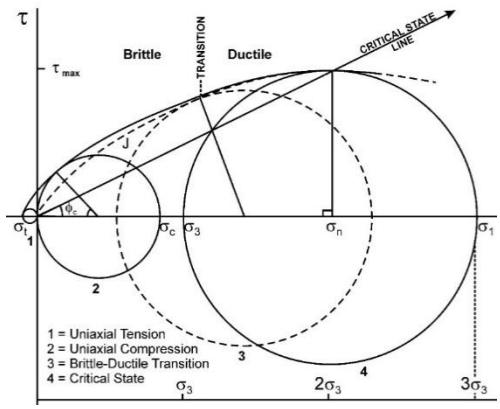

Figure 5. For estimating a lower-bound value of cohesion we can use the formulation that assumes a linear tangent between the tensile and compression circles, as in equation 3. (Barton, 1976).

$$c = 0.5(\sigma_t \cdot \sigma_c)^{0.5} \quad (3)$$

The logic behind an actually significantly *curved* failure envelope for intact rock was not only the consistent curvatures of numerous high pressure triaxial strength tests reported by Mogi, 1966 but also the finding of Singh et al. 2011 that the uniaxial strength Mohr circle is most frequently a virtual or actual tangent to the critical confining pressure σ_3 defining the maximum possible strength σ_1 in this figure from Barton, 1976.

The near-vertical cliffs in the weak materials illustrated in Figure 6 can be given assumed (saturated) strength values in the range σ_t =

Figure 6. Cliffs in weak materials: tuff in Cappadocia, Turkey and weak sandstone-limestone in Dorset, England. Judging by the surface roughness, these failures cannot be attributed to the opening of vertical jointing. (Such would have caused cliff failures long ago). Suitable estimates of (saturated) rock compressive and tensile strengths, partly based on test results from Aydan and Ulusay, 2003 could be the following: Top: Cappadocia cliff, 20m high next to the Christian church, tuff: σ_c = 5MPa, σ_t = 0.5MPa. Bottom: Burton cliffs, Dorset 40m high, weak sandstones and limestones. Estimated σ_c = 2MPa, σ_t = 0.2MPa.

0.2 to 0.5 MPa, and σ_c = 2 to 5 MPa for simplicity. Using these ranges of tensile and compression strengths, cohesional strengths (suitably rounded) as low as 0.3 and 0.8MPa can be estimated with the above linear lower-bound envelope (see Figure 5 caption).

The ratio of the compression to tensile strength Mohr circle diameters generates a presently assumed linear solution for internal friction angle φ as follows: $\sigma_c / \sigma_t = \tan^2(45° + \varphi/2)$. When the ratio of strengths is 10 as assumed for simplicity, this gives φ = 56°.

The lower-bound soil mechanics based relationship $h \geq 2c/\gamma \tan(45° + \varphi/2)$ following suitable adjustment of units (MPa x 1000 for conversion to kN/m^2 so that density can be expressed in kN/m^3) gives predictions of critical cliff heights of approximately 100m and 260m, i.e. far higher than the reality that is probably closer to a 20-60m range. The upper-bound solutions (equation 2) would be 200m and 520m.

Theoretical heights of mountain walls

We will now increase the assumptions about the strength of rock so as to attempt to address steep mountain walls, using the same unsuitable Mohr-Coulomb based formulations as outlined in Figure 4. Again, using deliberately simple numbers, and considering stronger sandstone and granite, we may assume the following approximate ranges of σ_t = 5 to 10MPa and σ_c = 50 to 100MPa.

The lower-bound solution for cohesion (assuming linear tangents with the σ_t and σ_c Mohr circles, Equation 3, Figure 5) gives estimates of cohesion for the stronger sandstone and granite of about 8 and 16MPa. These are too high to allow major rock avalanches, unless the vertical walls could be much higher. They usually cannot be, since failure occurs by different mechanisms, involving extension strain due to Poisson's ratio, and an anisotropic stress

Using the assumed higher strength values shown in Figure 7, and tensile/compressive strength ratios of 1/10 again, and the same lower-bound soil mechanics based relationship $h \geq 2c/\gamma \tan(45° + \varphi/2)$, following suitable adjustment of units (MPa

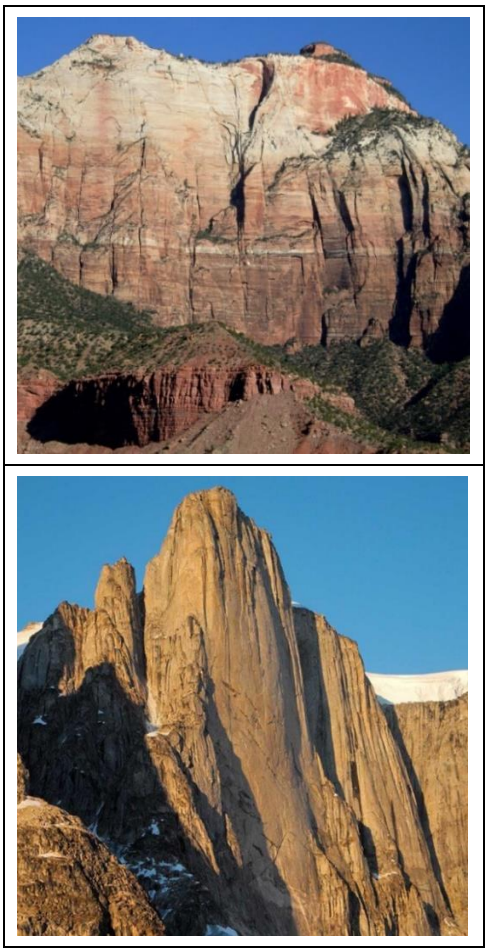

Figure 7. Mountain walls of almost record height in sandstone and granite are illustrated. Top: West Temple, 750m high, Zion, Utah formed of sandstones, with a conservatively assumed in situ saturated UCS = 50MPa. Bottom: Mirror Wall, 1,200m high, Greenland which we assume is formed of granite with a conservative in situ saturated UCS = 100MPa.

x 1000 for kN/m^2 and density expressed in kN/m^3), we obtain predictions of critical. mountain wall heights of approximately 2070m and 3700m, i.e. far higher than the reality (Figure 7) that is closer to a 750-1250m range. This time we have assumed rock densities higher than for the soft rocks: 2.5 and 2.8 t/m^3 or approximately 25 and 28 kN/m^3.

A new criterion for heights of cuttings, cliffs and mountain walls

When assessing the likely onset of failure in deep tunnels (Table 1 and Figure 1 show the details) we started by comparing maximum tangential stress and the uniaxial strength, based on the simplifying assumption of isotropic elastic behaviour – but applied nevertheless to explore the onset of fracturing. It was found (by Baotang Shen) that the ratio of tensile strength and Poisson's ratio (σ_t/ν) was a more correct description than the principal stress-induced fracture limit i.e. the well-known fraction of compression strength (0.4 σ_c).

Fracturing actually starts due to extension strain, but this fracturing may propagate in shear, creating classic log-spiral shear surfaces (Figure 1, centre) if stress levels are high enough. The latter is not possible behind steep mountain walls because stress levels are not high enough, as extension fracturing is likely to initiate when heights are much less.

Since the application of Mohr-Coulomb shear strength to the failure of rock cliffs and mountain walls is clearly not working for intact rock, because of the ultra-high cohesion as compared to soils, we will test the Shen σ_t/ν criterion 'in the vertical plane' (not along a potential shear plane), and simply equate it to an estimate of the major principal stress behind a vertical cliff or mountain wall. For simplicity we will assume $\sigma_{v\ max} = \gamma H$ where γ is the density. Equating the major stress and the failure criterion we obtain for the critical, maximum height H_c the simplest imaginable equation:

$$H_c = \sigma_t/\gamma\nu \qquad (4)$$

If we employ strength units of MPa, then the usual vertical stress estimate of $\sigma_v = \gamma H/100$ means that a multiplier of 100 is needed:

$$H_c = 100\,\sigma_t/\gamma\nu \qquad (5)$$

In Table 2 the Mohr-Coulomb derived maximum cliff and mountain wall height estimates (given in blue), are much too high compared with the extension-strain derived critical heights (given in red), based on the simple estimate of maximum vertical stress behind such walls. The red estimates are more in line with empirical evidence, but perhaps slightly high, suggesting that tensile strength is gradually reduced by the 'infinite' number of temperature cycles and wetting and drying cycles in the out-door environment on the surface of and behind these high rock walls. This cycling of temperature does not of course apply in the case of σ_t/ν application in tunnels.

Table 2. Comparison of Mohr-Coulomb derived and extension-strain derived critical vertical cliff and mountain wall heights with given assumptions.

Lower-bound estimate M-C: $h = 2c/\gamma \tan(45° + \varphi/2)$		
σ_t = 0.2 MPa, σ_c = 2 MPa	γ = 2.0 t/m^3	h = 103m
σ_t = 0.5 MPa, σ_c = 5 MPa	γ = 2.0 t/m^3	h = 258m
σ_t = 5 MPa, σ_c = 50 MPa	γ = 2.5 t/m^3	h = 2,067m
σ_t = 10 MPa, σ_c = 100 MPa	γ = 2.8 t/m^3	h = 3,690m

Extension strain based: $H_c = \sigma_t/\gamma\nu$		
σ_t = 0.2 MPa, σ_c = 2 MPa	ν = 0.2	H_c = 50m
σ_t = 0.5 MPa, σ_c = 5 MPa	ν = 0.2	H_c = 125m
σ_t = 5 MPa, σ_c = 50 MPa	ν = 0.25	H_c = 800m
σ_t = 10 MPa, σ_c = 100MPa	ν = 0.25	H_c = 1,430m

We can envisage that the slab failure sketched by Melosh, 2011 in Figure 8 would be a partial simulation of the σ_t/ν extension failure mechanism, when occurring in mostly intact massive rock.

The rock avalanche envisaged by Melosh in Figure 8 (bottom right) is likely to be a rare event, unless 'structure', as sketched in Figure 9 can develop over extended time, to make reduced areas of 'rock bridges' for shear failure to be finally possible, thereby counter-acting the usually too high cohesive strength of intact rock, as enumerated earlier. It is concluded that the rock avalanche mode is likely to be very rare in the case of massive hard rock, simply because shear stress will usually be insufficient to over-come the ultra-high cohesive strength of intact rock. The condition needed can perhaps be found in high mountains, and is fortunately rare.

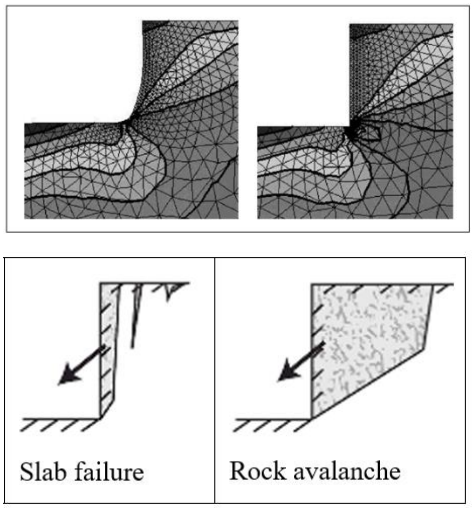

Figure 8. Top: Two examples of the principal (vertical) stress distribution in the case of near-vertical or vertical walls from Wolters and Müller, 2008. Bottom: Two of the failure modes in rock envisaged by Melosh, 2011

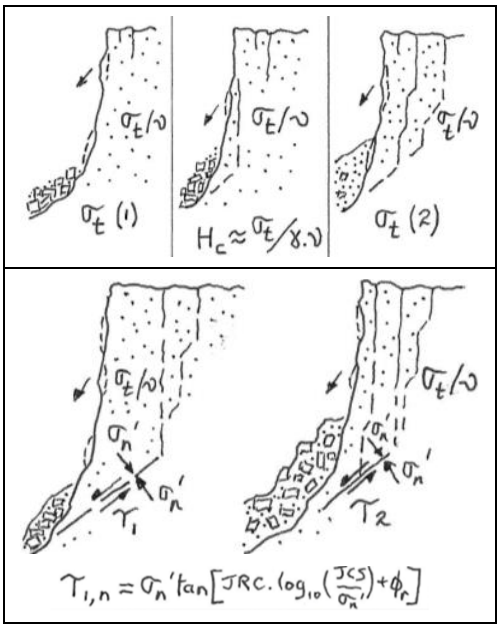

Figure 9. Sketches of slabbing mechanisms and joint propagation: responsible for large scale failures at the front of steep, high, mountain walls. Discontinuous, adversely oriented jointing that is under slope-induced shear stress might gradually propagate. JRC and JCS (and φ_r) might then play an important role. See 'whitest' plane in Figure 10.

The details sketched in Figure 9 include the implication that extension failures cause the slabbing mechanisms that slowly degrade largely unjointed mountain walls. Seasonal and daily temperature variations gradually degrade the tensile strength of the intact rock, while ice-wedging (and joint water pressure) will naturally be the dominant mechanism if discontinuous jointing is already present. El Capitan has all modes.

The lower sketch in Figure 9 explores the possible slow propagation of potential shear failure planes that could allow a rock avalanche to develop, despite a generally too high cohesive strength for the intact rock. Figures 10 and 11 illustrate two such mechanisms in different stages of development. In the case of El Capitan a major failure is extremely remote.

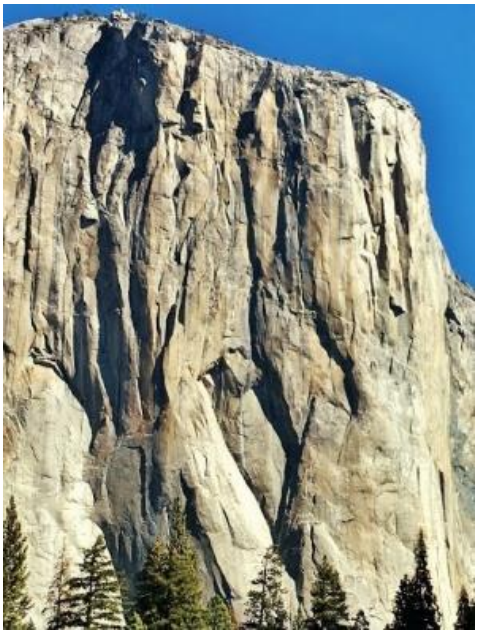

Figure 10. El Capitan in Yosemite, California which is the most climbed rock wall in the world, with a height varying from about 900-950m. (Record ascent times are just under 2 hours, and just under 4 hours for a unique free-solo by Alex Honnold).

It has been envisaged by those reviewing the origin of sheeting joints (e.g. Martel, 2017), that their frequent curvature, as seen for instance on the upper slopes of the Half Dome in Yosemite, is due to tensile stress

Figure 11. Holtanna, a 750m high monolith, in Dronning Maud's Land, Antarctica. The potential (imminent?) failure plane appears to dip at approx. 40 degrees. Extract from a Getty iStock image.

that can be generated by temperature cycling. This mechanism is not doubted. However, extension strain mechanisms can act very effectively on planar (i.e. mountain wall) surfaces as well, with the help of Poisson's ratio reacting to the marked stress anisotropy. The cycling of temperature is responsible for the gradual reduction of the tensile strength, and is an important geomorphological component of failure, aided by Poisson's ratio.

Figure 12. Alex Honnold ('Alone on the Wall', Honnold & Roberts, 2016) exploiting (assumed) extension fractures on Half Dome and El Capitan.

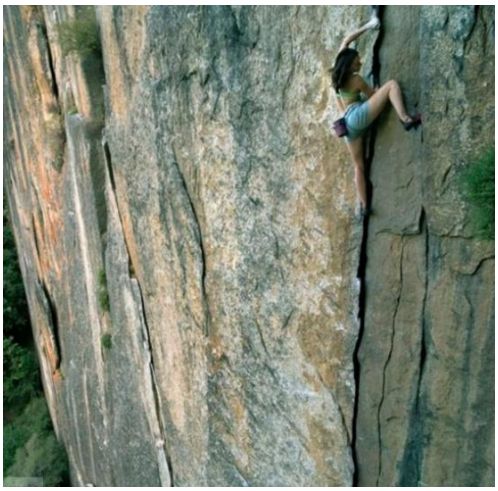

Figure 13. USA's free-solo ace Steph Davis exploiting extension fracture holds. (Davis, 2013. Learning to fly: An uncommon memoir etc.)

The world-famous free solo climbers Alex Honnold and Steph Davis from the USA may be utilizing extension fractures (rather than rock joints) in much of their free-solo climbing, because rock joints would be likely to have degraded a mountain too quickly when for instance the glacial support (as in cirques) retreated during the last formative ice-age. The extension crack surfaces can be continuous for 100's of meters, both horizontally and vertically, and can presumably develop in the third dimension if the slope-parallel horizontal stress is limited by a local free face. The long cracks are the focus of a large number (and size) of rock climber's camming devices for temporarily wedging in these cracks – but finger-tips, fingers, hands, clenched-fists, arms, feet and bodies are the 'cams' used by the free solo climbers, whose progress is faster without ropes. Refer to Davis, 2013, and Honnold and Roberts, 2016 for numerous very fine photographs of planar extension fractures.

Complications from multi-component failure-modes

Before leaving the proposed extension failure mode, which has been shown in Table 2 to more accurately describe the limiting heights of cliffs and mountain walls, it is necessary to address another class of slope/wall stability conditions. It has already been hinted that well-developed jointing will not generally be compatible with (semi-) stable steep slopes, because degradation involving failure along the joints would likely be so fast that the front-lying screes of joint-delineated blocks would have prejudiced the long-term existence of the mountain wall (or sea cliff).

For example, the scree of fallen blocks might be hundreds of meters in vertical extent, while the remaining mountain has become a residual and steadily reducing cliff now only 50 to 100m high. There are many examples of such degraded walls, aided by ice-wedging, water and water pressure, especially in well-jointed (Jn ≥ 9, three joint sets or more) hard quartzites.

In this section of the paper we will briefly address the stability and (perhaps) ultimate failure of slowly degrading mountain walls, of which there are some well-known examples in the glaciated fjords and steep valleys of Norway. They have presumably degraded at varying rates (faster at first) following the retreat of the ice. A longer-term pseudo-stability depends on the presence of less developed jointing and depends on significant 'stretches' or 'bridges' of intact rock. A fine example from Norway is shown later. Stability also depends on the relative absence of clay-filled features, at least an absence of adversely oriented discontinuities of this type.

The three strongest shear strength components illustrated in Figure 14 symbolically involve the strength of intact rock (the 'bridges'), followed by shearing along these newly created surfaces which are likely to have high JRC and high JCS (≈ UCS) and $\varphi_r \approx \varphi_b$ due to a likely lack of weathering. These components were introduced in Barton, 1973 and refined in Barton and Choubey, 1977. The third shear strength component is the rock joints, which

are likely to be favourably oriented if there is pseudo-stability, or not very continuous, because they will tend to have significantly reduced values of JRC, JCS and φ_r When performing distinct element modelling with partially developed (even numerically-glued) jointing, it may be important to ensure that the shear strength input data for the continuous portions of the joints are suitably scaled for block size. The latter may be very large in the case of pseudo-stable slopes/mountain walls, so scale-effects will be a source of potential error.

Note that the shear stiffness k_s of joints, which is doubly scale-dependent (peak strength reduction and displacement-to-peak increase) may be as low as 1-5MPa/mm. In fact at low normal stress levels it can be < 1MPa/mm. The normal stiffness k_n of rock joints is much higher and is less prone to scale effects (Bandis et al., 1983, Barton, 2006).

The shear resistance of the rock mass through which a steep slope is artificially cut (or glacially gouged) can cause the new slope to fail immediately when glacial support is lost, or to be moderately stable if there are no continuous failure surfaces along the existing joint sets. In a rock engineering context, bolting and/or anchoring during downwards excavation can obviously ensure stability.

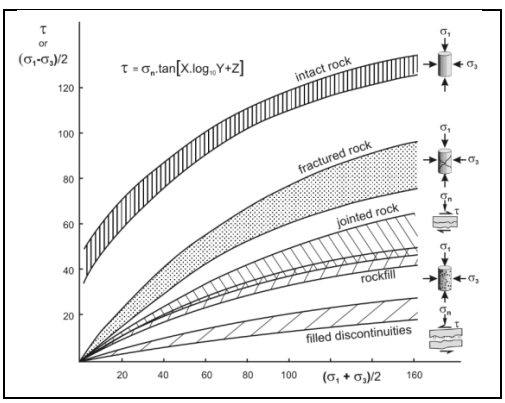

Figure 14. The four principal shear strength components of jointed rock masses. If rock joints are non-planar, three will be non-linear curves.

A large rock slope, for instance an open pit, may depend for its stability on all four of the illustrated strength components: 1. Strength of intact 'bridges'. 2. Shearing (or not) on these new, fresh, rough surfaces. 3. Mobilization (or not) along an already existing joint plane. 4. Finally the usually limited strength of any clay-filled discontinuities or faults, which have the lowest shear stiffness (Barton, 1999, 2013).

Table 3. Non-linear approximations to the three shear strength components: intact rock, new fractures, and rock joints. Barton, 1976, 2013.

X	Y	Z
50	$\left(\frac{\sigma_1-\sigma_3}{\sigma_n}\right)$	ϕ_c
20	$\left(\frac{\sigma_1-\sigma_3}{\sigma_n}\right)$	ϕ_b
JRC	$\left(\frac{\sigma_1-\sigma_3}{\sigma_n}\right)$	ϕ_b
or	$\left(\frac{JCS}{\sigma_n}\right)$	ϕ_r

The four potential strength components (which must include clay-filled discontinuities) might, if one was close-by during failure, be heard as 'bang', 'crunch', 'scrape', 'swoosh' : i.e. a progressive and process-dependent shear failure. Neither M-C (linear) 'c + σ'_n tan φ', nor H-B (non-linear) 'c + σ'_n tan φ', but 'c <u>then</u> σ_n tan φ' – or the above x, y, z non-linear equivalents (# 1, 2, 3 and 5) are likely to be most correct, and would be consistent with the observation (and monitoring) of progressive failure. Computational simplicity (conventional linear M-C) or GSI-based H-B provides 'solutions', but the reality is often different.

A famous tourist attraction in S.W. Norway, 600m above the Lysefjord is called *Prekestolen* ('pulpit'). A major tension crack and a back-wall plane of weakness 'combine' to throw a likely elevated shear and vertical stress onto a presently intact 'toe' somewhere near the white arrow about 200m below the 'lectern'. The big question in relation to the theme of multi-component shear resistance: will there be initial shear

failure or extension failure: c + tan φ, c then tan φ, or a likely $\sigma_t/\gamma v$? The principle 'rock engineering' components (joint planes) of Prekestolen are shown in Figure 15 and include an unusual cyclic 'micro-loading' from a widely varying number of tourists.

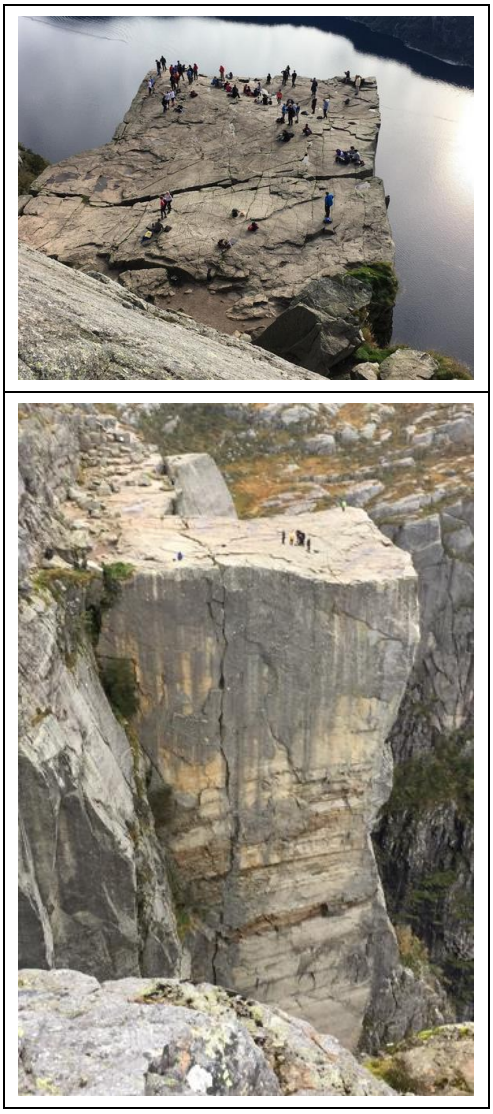

Figure 15. a, b, c, d. Prekestolen in S.W. Norway, 600m above the Lysefjord. Three of these photographs were kindly provided by Katrine Mo from a comprehensive MSc. thesis concerning the stability of this challenging 'monolith'.

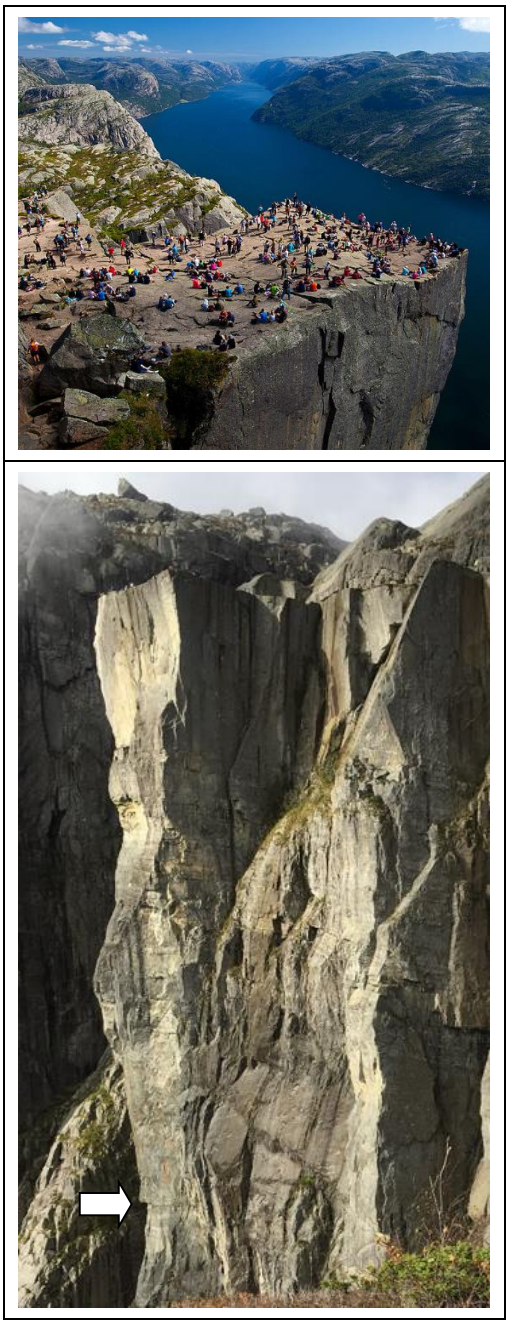

The white arrow in the above photograph is located in a region where the vertical stress may be strongly concentrated, due to the jointing through the upper levels of rock.

The limited height of the world's highest mountains

There are fifteen mountains in the world with heights in the rarified range of 8 to 9km. The highest of these is Everest at approximately 8,848m. An extract from a Wikipedia photograph is shown in Figure 16.

Since we are concerned with the ultimate strength of rock one can pose the question: why are the highest mountains no higher than 9km? Have mountains ever been higher than this during the earth's history? Since plate tectonics has been at work for a very long time, and contrary glacial processes during 'infinite' millenia also, one can perhaps assume that the extensive 'empirical evidence' that we see today is also a reflection of what has been in the distant past. The strength of rock has little reason to have changed either, though it could be higher today, if the geothermal gradient had declined significantly.

In a well-known article written by Terzaghi (1962) near the end of his life: '*Stability of steep slopes on hard unweathered rock*', a simple formulation of critical slope height was suggested: $H = q/\gamma$, where the uniaxial strength of rock and the vertical stress caused by its density are compared. The assumed vertical stress is estimated to be γH (or $\gamma H/100$ if using familiar MPa units as in rock mechanics). One can also use units kN/m^2 and kN/m^3 for the rock strength and density.

This formula was not evaluated in the section concerning limited cliff heights and mountain walls since it (also) produces a strongly exaggerated result, and Terzaghi was quick to point out in the same 1962 article that the adverse effect of jointing must be the reason that 'critical slope heights' were not in practice as high as this formula was suggesting. The reason (besides jointing) is that in the case of massive intact rock, there are alternative mechanisms of rock failure: possibly even shear failure when stress levels are high.

Figure 16. Mount Everest, 8,864m (Wikipedia photo extract). Note that the peak of Everest is immediately behind the peak showing possible curved 'shear-planes'. (This cannot be tilted bedding with such a huge variation in thickness.).

Misuse of the 'Terzaghi' formula: $h_c = \sigma_c/\gamma$ (equation 6) gives an apparently correct answer for maximum mountain heights (e.g. 100 x 250/2.8 = 8.9km). The problem is that it has to be the *confined strength* of rock at 9 km depth, and this is much too high.

$$h_c = \sigma_c/\gamma \qquad (6)$$

Application of a typically high value of uniaxial compression strength of rock in the case of ultimate mountain height estimation is a 'popular' method that is also shown in a Google 'chat-site'. The problem is that the rock involved in 'stabilizing' the vertical effective stress generated by the mountain, cannot possibly be the *unconfined* strength at e.g. 9km depth. It must be the *confined* compressive strength. We would then have impossible 30km high mountains.

Correct logic suggests that mountains are of 'limited' height due to a lower (critical state) shear strength, which may also be approximately 200-250 MPa. Inspection of Figures 18 and 19 gives simple confirmation that the indicated value of σ_1 (see right-hand side of largest Mohr circle) would be much too high in relation to σ_c. On the other hand, the maximum shear strength is of similar magnitude (or equal) to the uniaxial strength. (See Barton, 1976 and Singh et al. 2011, and the recent article by Shen et al. 2019). Observation of the strong curvature

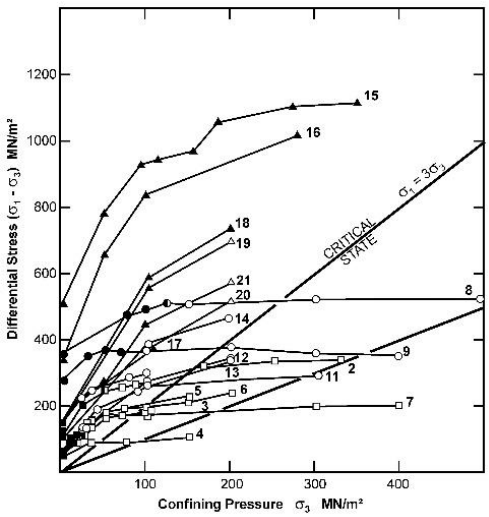

Figure 18. The strong curvature of this and other sets of high-pressure triaxial data from Mogi, 1966 was the direct reason for a critical state proposal.

of the shear strength of intact rock at high confining pressure, as reviewed by Barton, 1976 with this example from Mogi, 1966 (Figure 18) was the reason for proposing a critical state maximum possible shear strength (Figure 19).

Since then, an important study of more than 1,000 triaxial tests was performed by Singh et al. 2011, who verified that the majority of rocks exhibited the close proximity, if not the equality, of the UCS Mohr circle and the critical confining pressure needed to reach the critical stress (see σ_c and σ_3 sides of adjacent Mohr circles in Figure 19). Since σ_c is approximately numerically equal to τ_{max} (note the equality of diameter and radius in Figure 19), we have an explanation for the high, but none the less limited shear strength of potential failure planes deep below the world's highest mountain chains.

The consequences of the strong curvature of shear strength envelopes, actually stronger curvature than that of the Hoek-Brown criterion for intact rock, have been further investigated by Shen et al. 2018, who demonstrated with the FRACOD fracture mechanics code (Shen et al. 2013) that a somewhat larger volume of rock would be fractured as a result of tunnel siting at 1 or 2km depth, as compared to the fracturing depth modelled with conventional models of shear strength.

Shen managed to formulate relatively simple equations with recognisable input parameters, to describe both the tensile and compressive side of the non-linear shear strength. Recently we gave examples of typical strength envelopes (Shen et al. 2019) as illustrated in Figure 20. Approximate (numerical) conversion by Shi to the format σ_1 versus σ_3 shown in Figure 21, reinforces the impossibility of using the c*onfined* compressive strength of rock to estimate mountain height limits.

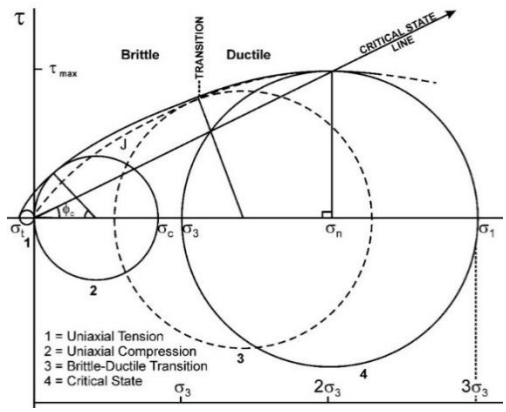

Figure 19. The critical state suggestion of Barton, 1976. Note the proximity of UCS (or σ_c) and the critical confining pressure σ_3. Singh et al. 2011 found that σ_c and σ_3 had equal or very similar magnitude.

Shen and Shi are responsible for the generation of the four example strength envelopes shown in Figure 20. These were evaluated based on Shen's recent formulations for the tensile and compressive regions of the strength envelope. The input data was suggested by the writer, so that the critical state theory of 1976 could be more easily understood as a logical and very simple strength criterion. Note the touching Mohr circles for each set.

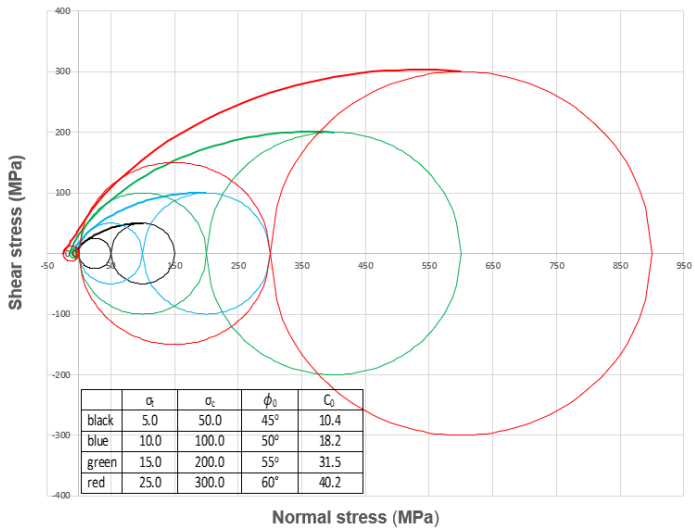

Approximate nonlinear strength criteria with critical state for intact rocks.

Shen, Shi, Barton, 2019

$$\phi = \phi_0 - (45° - \phi_0)\frac{\sigma_n}{\sigma_t}$$

$$c = c_0 + (\sigma_t - c_0)\left(\frac{\sigma_n}{\sigma_t}\right)^2$$

$$\phi = \phi_0\left(1 - \sqrt{\frac{\sigma_n}{2\sigma_c}}\right)$$

$$c = c_0 + (\sigma_c - c_0)\frac{\sigma_n}{2\sigma_c}$$

Figure 20. Example non-linear shear strength envelopes developed from four sets of input data (see inset table) using the tensile-region and compression-region equations recently suggested by Shen.

When the shear strength envelopes are converted to the form σ_1 versus σ_3 the impossibility of mountain height estimation using equation 6 is further emphasised by the high values of ($\sigma_1 - \sigma_3$) at relevant sub-mountain depths of 8 to 10km.

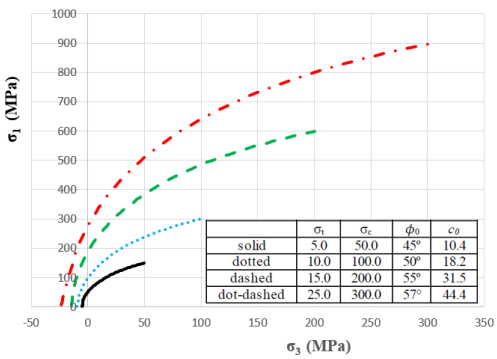

Figure 21. The confined compressive strength for rocks at e.g. 9km depth, where the confining pressure σ_3 might be of the order of 2.8 x 9,000/100 = 250 MPa, or perhaps higher due to the tectonic thrust against the Himalayas, where most of the highest peaks are found. This suggests that $\sigma_1 - \sigma_3$ will be much too high to explain 'only' 8 to 9km maximum mountain heights. Shen et al. 2019.

Some brief observations about karst

This paper has so far been devoid of comments about engineering and geotechnical problems in karstic regions. A relatively limited involvement in such engineering challenges, such as a single leaking surge tunnel, and opposite ends of a TBM tunnel, does not qualify for extensive comment here, Nevertheless, a fascination with the phenoma of karst, such as the relative lack of soil on mountain slopes in limestones, and the remarkable local permeabilities, have not passed unnoticed, and three or four photographs from southern Greece will now be commented, to emphasise simple lessons learned.

As all involved with karst know well, the *usual range* of magnitudes of geotechnical parameters, such as three orders of magnitude for *shear strength* and *deformability*, and at least six orders of magnitude for *permeabiity*, are made nonsence of in karstic terrain.

Figure 22. A limestone hand specimen with four jointed sides and a solution channel through each. Turned appropriately, a karstic 'joker' is revealed.

Figure 23.. A minor demonstration of outflow from karstic channels in a hillside, from Altamira in southern Greece, following a rain-storm at Prof. Stavros Bandis's mountain, book-writing retreat.

For instance, an exceptionally high rock mass permeability of 10^{-4} m/s (i.e. an almost impossible to measure 1,000 Lugeons, or 1,000 litres/min/'per meter' of borehole) could occasionally be the equivalent of 10^{1} or even 10^{2} m/s in the case of karst-cavern inrush into tunnels, 'adding' four or five orders of magnitude to 'k'.

Back-filling with concrete and pre- or post-injection might be a tunnelling solution if the karstic void is small enough, as in Figure 23, but only when in-flow has almost stopped, which might be a very long time. 'Expect the unexpected' would seem like the best advice when tunnelling in karstic terrain, and over-lapping multiple probe-drilling ahead of TBM through limestone stretches is always advised,

Sudden inflows of 1 and even (river-scale) $4m^3$/sec may cause one year or more tunnelling delays, as experienced in the Zagros mountains in Iran. Occasionally a bridge might be needed to transport a TBM back into rock on the other side of a cavernous void. Inundation by fines, or drowning by water are both possible, and are sometimes experienced in combination or succession.

Conclusions

1. Tensile strength and Poisson's ratio explain the limited maximum heights of cliffs and steep mountain walls, and the origin of planar sheeting joints. A range of maximum heights from 20m in tuff, 100m in chalk, 750m in sandstone, to 1,300m in granite can be sensibly quantified by considering failure caused by extensional strain in each case. Mohr-Coulomb shear strength parameters give incorrect results for intact rock, in the context of steep slopes.

2. There are parallels in the world of deep tunnels in hard rock. The widely quoted critical tangential stress of 0.4 x UCS that may be reached by deep hard-rock tunneling can be replaced by the ratio σ_t/ν, representing initial tensile failure which is mobilized by extensional strain. These two ratios are numerically equivalent. At higher stress levels, tensile fractures may propagate in unstable shear, meaning potential rock bursts.

3. Shear strength and tensile strength (ably assisted by Poisson's ratio) are inevitably the weakest links in 'high-stress' structural geology and in 'low-stress' geomorphology, respectively.

4. Rock slopes with discontinuous rock joints may reach failure if several shear strength components are mobilised/overcome one-by-one in a progressive manner. Recall: crack, crunch, scrape, swoosh as a reminder of a non-Mohr-Coulomb event.

5. The highest mountains of 8 to 9km are most likely to be limited by maximum possible, critical state shear strength, not by compressive strength, because the confined strength of competent mountain-forming rock is at least two times too high. Mountains cannot be 20-25km high.

6. The usual three or more orders of magnitude range of geotechnical parameters, such as shear strength, or deformation modulus, or tunnel deformation, with perhaps six orders of magnitude range for permeability are made to look minor by karst inrushes to tunnels. The usual log-scale permeability units of m/s may experience a quantum leap, from negative to positive components.

References

Addis, M.A., Barton, N., Bandis, S.C. and Henry, J.P. 1990. Laboratory studies on the stability of vertical and deviated boreholes. *65th Annual Technical Conference and Exhibition of the Society of Petroleum Engineers*, New Orleans, September 23-26, 1990.

Aydan, Ö. and R. Ulusay, 2003. Geotechnical and geoenvironmental characteristics of man-made underground structures in Cappadocia, Turkey. *Engineering Geology,* 69, 245-272.

Bandis, S., Lumsden, A.C. and Barton, N. 1983. Fundamentals of rock joint deformation. *Int. J. Rock Mech. Min. Sci. and Geomech. Abstr.* Vol. 20: 6: 249-268.

Barton, N. 1973. Review of a new shear strength criterion for rock joints, *Engineering Geology*, Elsevier, Amsterdam, Vol. 7, pp. 287-332. Also NGI Publ. 105, 1974.

Barton, N., Lien, R. and Lunde, J. 1974. Engineering classification of rock masses for the design of tunnel support. *Rock Mechanics*. 6: 4: 189-236.

Barton, N. 1976. The shear strength of rock and rock joints. *Int. Jour. Rock Mech. Min. Sci. and Geomech. Abstr.,* Vol. 13, No. 9: 255-279.

Barton, N. & Choubey, V. 1977. The shear strength of rock joints in theory and practice. *Rock Mechanics* 1/2:1-54. Vienna: Springer.

Barton, N. 1999. General report concerning some 20th Century lessons and 21st Century challenges in applied rock mechanics, safety and control of the environment. *Proc. of 9th ISRM Congress,* Paris, 3: 1659-1679, Balkema, Netherlands.

Barton, N. 2013. Shear strength criteria for rock, rock joints, rockfill and rock masses: problems and some solutions. *J. of Rock Mech. & Geotech. Engr*., Elsevier 5(2013) 249-261.

Barton, N. and Grimstad, E. 2014. Q-system - an illustrated guide following forty years in tunnelling. 43 p. *www.nickbarton.com*.

Barton, N. and Shen, B. 2017. Extension failure mechanisms explain failure initiation in deep tunnels *and* critical heights of cliff faces and near-vertical mountain walls. *US Rock Mech. Symp. San Fransisco,* ARMA17-686, 20p.

Davis, S. 2013. *Learning to Fly: An Uncommon Memoir of Human Flight, Unexpected Love, and One Amazing Dog.* A Touchstone Book, Simon & Schuster, New York, 292p.

Grimstad, E. and Barton, N. 1993. Updating of the Q-System for NMT. *Proc. of Int. Symp. on Sprayed Concrete – Modern Use of Wet Mix Sprayed Concrete for Underground Support,* Fagernes, 1993, Eds Kompen, Opsahl and Berg. Norwegian Concrete Association, Oslo, 46-66.

Honnold, A. and D. Roberts, 2016. *Alone on the Wall.* W.W. Norton & Company, New York. 248p.

Martel, S.J. 2017. Progress in understanding sheeting joints over the past two centuries. *Jour. of Structural Geology*, Elsevier, 94, 68-86.

Martin, C.D., Kaiser, P.K. and McCreath, D.R. 1998. Hoek–Brown parameters for predicting the depth of brittle failure around tunnels. *Can. Geotech. J.* 36, 136-151.

Melosh, H.J. 2011. *Planetary surface processes*. Cambridge University Press, Cambridge.

Mo, K. 2018. Stability Analysis of Preikestolen. M.Sc., Engineering Geology, *NTNU*, Trondheim.

Mogi K. 1966. Pressure dependence of rock strength and transition from brittle to ductile flow. *Bulletin of Earthquake Research Institution,* 44: 215-32.

Shen, B., Stephansson, O. and Rinne, M., 2013. *Modelling Rock Fracturing Processes: A Fracture Mechanics Approach Using FRACOD.* Springer, 173p.

Shen, B., Shi, J. and N. Barton, 2018. An Approximate Non-Linear Modified Mohr-Coulomb Shear Strength Criterion with Critical State for Intact Rocks. *Journal of Rock Mech. and Geotech. Eng*. 10 (2018) 645-652.

Shen, B., Shi, J. and N. Barton, 2019. Graphic examples of a logical non-linear strength criterion for intact rock. Rock Mechanics and Rock Engineering. In press.

Singh, M., Raj, A. and B. Singh. 2011. Modified Mohr-Coulomb criterion for non-linear triaxial and polyaxial strength of intact rocks. *Int. J. Rock Mech. Min. Sci.,* 48(4), 546-555.

Stacey, T.R. 1981. A simple Extension Strain Criterion for Fracture of Brittle Rock. *Int. J. Rock Mech. Min. Sci. & Geomech. Abstr.* 18, 469-474.

Terzaghi, K. 1962. Stability of steep slopes on hard unweathered rock. *Geotechnique* 12:251-263.

Verruijt, A. 2001. *Soil Mechanics*. Delft University of Technology, The Netherlands.

Wolters, G. and Müller, G. 2008. Effect of cliff shape on internal stresses and rock slope stability. *J. Coastal Res.* 24(1), 43–50.